Scanning Microscopy

Volume 1 | Number 1 Article 6

11-28-1986

Recent Advances in Scanning Electron Microscope Cathodoluminescence Assessment of GaAs and InP

C. A. Warwick
Royal Signals and Radar Establishment

Follow this and additional works at: https://digitalcommons.usu.edu/microscopy

Part of the Life Sciences Commons

Recommended Citation
Warwick, C. A. (1986) "Recent Advances in Scanning Electron Microscope Cathodoluminescence Assessment of GaAs and InP," *Scanning Microscopy*: Vol. 1 : No. 1 , Article 6.
Available at: https://digitalcommons.usu.edu/microscopy/vol1/iss1/6

This Article is brought to you for free and open access by the Western Dairy Center at DigitalCommons@USU. It has been accepted for inclusion in Scanning Microscopy by an authorized administrator of DigitalCommons@USU. For more information, please contact digitalcommons@usu.edu.

Scanning Microscopy, Vol. 1, No. 1, 1987 (Pages 51-61)
Scanning Microscopy International, Chicago (AMF O'Hare), IL 60666 USA

0981-7035/87$3.00+.00

RECENT ADVANCES IN SCANNING ELECTRON MICROSCOPE CATHODOLUMINESCENCE ASSESSMENT OF GaAs AND InP

C A Warwick*

Royal Signals and Radar Establishment
St. Andrews Road, Malvern, U.K.

(Received for publication May 04, 1986, and in revised form November 28, 1986)

Abstract

The capabilities of the cathodoluminescence mode of the scanning electron microscope are reviewed, with particular reference to the low temperature wavelength dispersive system in the author's own laboratory. The design of the luminescence collection optics is highlighted. The interpretation of the luminescence spectra is discussed in terms of the physics of radiative recombination. We offer some solutions to some of the main experimental problems with illustrations drawn from two case studies. The first is a study of the elimination of dopant striations in dislocation-free germanium doped indium phosphide and the second an analysis of the causes of threshold voltage scattering in GaAs Schottky-gated field effect transistors. Future directions of the technique are speculated upon.

KEYWORDS: Scanning electron microscope, cathodoluminescence, gallium arsenide, indium phosphide.

*Address for correspondence:
RSRE, St Andrews Road, Malvern, Worcs, WR14 3PS, UK.

Phone No. +44 6845 2733

Introduction

Cathodoluminescence (CL), the light generated by electron beams ("cathode rays"), was first observed in diamond by Crookes (1879) over a hundred years ago. Indeed, electron beams provide a convenient source of flood excitation for many luminescence studies, especially where the material's band gap is too large for photo-excitation by a laser beam. However, it is the spatial resolution and imaging capabilities of the scanning electron microscope (SEM) which have brought CL into widespread use in semiconductor assessment, where small devices and microscopic homogeneity of materials are important, and the very high impurity sensitivity ($\ll$ 0.1 part per million atomic) of a luminescence technique is required.

The aim of the present paper is to promote SEM CL by reviewing the equipment needed, the difficulties to be overcome and the results which can be achieved by the technique. Examples from the author's laboratories are given.

Apparatus

The apparatus, capabilities and typical use of the four main levels of sophistication of SEM CL are given in Table 1. These techniques have been reviewed in detail by Yacobi and Holt (1986) and Hasenrath and Kubalek (1982). We use the term wavelength dispersive CL (WDCL) to signify a system with a dispersive element, such as a grating monochromator, by analogy with the wavelength dispersive x-ray (WDX) technique. Similarly luminescence decay measurements are called time dispersive (TD) CL.

As we discuss later on in this paper, further widening of the use of SEM CL techniques awaits the development of automated interpretation and correction software, analogous to the ZAF (atomic number Z, Absorption and Fluorescence) corrections in energy dispersive X-ray(EDX) and WDX analysis. The lack of this software makes interpretation of SEM-WDCL a specialized and skilled job, so demand for systems is limited. As a result no complete package of equipment is available. Table 2 lists the components of the author's own system. The crucial part of any CL system is the collection optics which in the present case were designed

Symbol Table

Symbol (with variants)	Description (with variants)	Unit
T	Absolute temperature	K
k	Boltzmann's constant	$J\ K^{-1}$
$\underline{k}$	Electronwave vector	m
$\overline{a}_0$ (a)	Bohr radius (effective Bohr radius)	m
n (n_0;$n(t)$;n_e)	Carrier concentration (in dynamic equilibrium; as a function of time; electron concentration)	m^{-3}, cm^{-3}
N (N_D;N_A)	Impurity concentration (donor concentration; acceptor concentration)	m^{-3}, cm^{-3}
E (E_g)	Energy of electron or photon (band gap energy)	J, eV
ΔE	Energy change	J, eV
h	Planck's constant	J s
$\hbar$	$h/2\pi$	J s
ν (ν_1; etc)	Photon frequency (first process; etc)	Hz
c	Speed of light in vacuo	$m\ s^{-1}$
n_{air}	Refractive index of air	-
λ_{air}	Light wavelength (in air)	m, µm
A (A°;A^-;A_2 etc)	General acceptor (neutral;ionized; second type etc)	-
D (D°;D^+;D^*)	General donor (neutral;ionized; excited)	-
e^-	Electron in conduction band	-
e	Charge on electron	C
h^+	Hole in valence band	-
Si_{As} (Si_{Ga}) etc	Silicon (etc) on an As (Ga) site	-
X	Exciton	-
R_i (R_{io})	Recombination rate through ith channel (in dynamic equilibrium)	Hz
a_i	Recombination strength of ith channel per centre	$m^6\ s^{-1}$, $cm^6\ s^{-1}$
c_i	Concentration of ith channel centres	m^{-3}, cm^{-3}
G	Minority carrier injection rate	Hz
i	Index integer of recombination channel	-
j	Number of recombination channels	
t	Time	s
τ	Luminescence decay time constant	s
I_i (I_{io})	CL intensity of ith peak (in dynamic equilibrium)	-
ε_0	Permittivity of free space	$F\ m^{-1}$
ε_r	Relative dielectric constant	-
m (m_e;m_h)	Effective mass (electron;hole)	kg
m_0	Free electron rest mass	kg
E_D; E_A	Ionization energy (donor;acceptor)	J, meV
ω (ω_1,ω_2 etc)	Peak width	m,µm,nm

Table 1

Four Main Levels of Sophistication of SEM-CL

Level	Name	Equipment	Capability	Applications
A	SEM-CL	SEM + light collector and detector	"Total-light" imaging ~3 µm resolution	Dislocation density and distribution Homogeneity Surface damage
B	SEM-WDCL	+ improved collector + monochromator	+ monochromatic images + micro luminescence spectra eg selected devices	+ alloy composition and uniformity e.g. InGaAsP
C	Low temperature SEM-WDCL	+ cryogenic specimen stage	+ impurity/ dopant spectra semi-quantitative with skill	+ impurity/dopant distribution
D	Low temperature SEM-TDWDCL	+ fast beam blanking + luminescence decay time nucleonics	+ micro luminescence decay time	+ quantitative impurity distribution

Table 2

List of Components in the RSRE SEM-WDCL Apparatus

Component	Details
SEM	Cambridge Instruments, S150 mkl with LaB_6 electron source
Beam blanker	Lintech Instruments, knife edge beam blanker
Cryogenic specimen Stage	Oxford Instruments Liquid He ~ 6K kT ~ 1 meV
Collection optics	In-house designed and built
Monochromator/ Computer drive	Bentham Instruments/Link Systems Monochromator Resolution ~0.5 meV Dual use as EDX Computer controlled
Detectors	0.3 µm → 5.5 µm GaAs, S1 [PMT] Ge (North Coast) InAs (Judson) InSb (Judson) PbS (SBRC) [solid state]

and built in-house.†

The optics consist of a half parabolic mirror, a light guide, a vacuum window, a lens and a movable 45° mirror. The half parabolic mirror has its axis in a horizontal position. The specimen surface is horizontal and at the focus of the mirror. A small hole, with its axis vertical and co-linear with the electron beam is machined in the mirror. The light is guided out through the light guide through a vacuum viewport window. The parallel beam of light is then focussed with a lens onto the monochromator slits. A 45° mirror can be interposed between the lens and slits to reflect the light onto the photomultiplier for "total light" experiments.

The system has proven to be very effective, and a list of its features is given in Table 3. A block diagram of the author's SEM-WDCL system is shown in Figure 1.

Quantitative Interpretation of Low Temperature SEM-WDCL Spectra

The low temperature luminescence spectrum of semiconductors is a sensitive function of the nature and quantity of impurities, dopant and point defects present, as well as the alloy composition of, for example, InGaAsP or AlGaAs. The spectrum is radically altered by amounts of impurity etc. in the parts per billion range.

† Details available from Defence Technology Enterprises, RSRE, St Andrews Road, Malvern, Worcs, WR14 3PS, UK.

This gives the microscopic WDCL technique a large potential advantage over secondary ion mass spectrometry (SIMS) by two orders of magnitude in sensitivity (or more in certain important cases such as carbon in GaAs, which is very difficult to detect by SIMS). There are a number of other advantages: 1) SEM-WDCL detects electrically active impurities in the host crystal and therefore need not be affected by spurious surface contamination. 2) Electrically different, but chemically identical defects, eg. silicon on an arsenic site, Si_{As}, and Si_{Ga}, give different CL peaks, enabling amphoteric doping to be studied microscopically. 3) Native defects such as As can be detected; these defects are technologically important, but difficult to measure chemically.

However, wider application of SEM-WDCL is currently limited by the difficulty in quantifying the spectra. The interpretation of luminescence spectra is more complex than EDX or WDX spectra because the intensity of a particular peak is not proportional to the concentration of the related defect but (approximately) to the product of the concentration and the minority carrier lifetime. This is because luminescence is a competitive process (a simple illustration of this is given in Appendix 1). If we can measure both the microscopic luminescence decay time and the intensity (e.g. with SEM-TDWDCL) and can apply corrections for Mixed level injection, Absorption and Surface recombination (MAS, analogous to ZAF, corrections) then we can quantify the concentration, with an accuracy dependent on

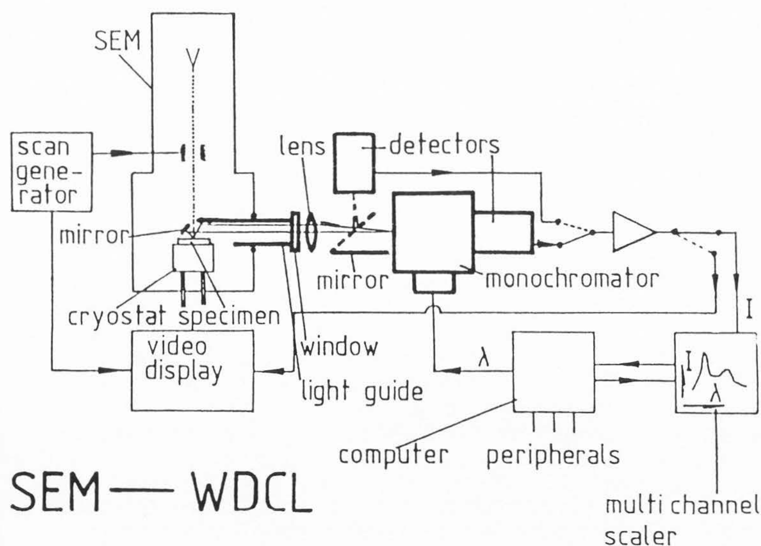

Figure 1. Block diagram of the low temperature SEM-WDCL system.

Table 3

Features of the RSRE CL Collection Optics

1. Very high collection efficiency into narrow monochromator slits

2. Short working distance (low spherical aberration, large probe current): 12 mm

3. Controlled field of view
- wide for low magnification
- narrow for spectra

4. Very wide wavelength range 0.3 m to 5.5 m

5. Horizontal output in vertical SEM

6. Alignable

7. External XY alignment of optics with respect to electron beam

8. Retractable for EDX/SE

9. No materials that scintillate are used.

the sophistication of the physics in the software. Mixed level injection means that the excess carrier concentration is greater than the ionized impurity concentration in some places (i.e. near the electron probe) and less than the ionized impurity concentration in others (i.e. a few micrometers away from the electron probe). The TDWDCL hardware has been developed by a small number of workers and has been reviewed by Hastenrath and Kubalek (1982).

If time dispersive measurements are not available then other forms of interpretation must be used. Many such methods are found in the photoluminescence (PL) literature. Peak intensity ratios, peak widths, peak energies and straightforward peak intensities have been used. However, Swaminathan et al (1982) showed that, in GaAs at 5.5K, the intensity of the 1.51 eV donor related peak was only weakly related to the chemical concentration of donors measured by SIMS. Kyser and Wittry (1964) found a similar poor correlation at 300K. This is due to lifetime variation (e.g. due to varying deep level concentration) from sample to sample (Hwang, 1972). For a range of samples with a given luminescence intensity, the chemical concentration of donors varied by about one order of magnitude. Thus, the intensity alone is a poor measure of concentration.

Peak height ratios can often eliminate the need for knowledge of the lifetime (provided only concentration ratios are required), but only if the lifetimes of the two processes are equal (i.e. same rate limiting carrier type) and carrier capture is the rate limiting step. Varying the excitation intensity while observing the ratio of emission intensities has often been used in the PL literature and is a very valuable method (Swaminathan et al, 1982; Nam et al, 1977; Kikuta et al, 1984; Pickering et al, 1983; Kamiya and Wagner, 1983).

At room temperature the WDCL spectra are thermally broadened. The peak width corresponds to the energy spread of the carriers, this is ~3/2 kT where T is the absolute temperature and k is Boltzmann's constant. The value of the expression is ~39 meV at 300K, ~10 meV at 77K and ~0.5 meV at 4K. At low temperatures and for impurity related energy levels close to a band energy (ie. shallow levels) the peak width is limited by Mott broadening, which is due to the wavefunction overlap of charge carriers localized on impurities. The amount of broadening is proportional to $aN^{1/3}$, where a is the ground state "Bohr radius", modified with appropriate dielectric constants and effective masses, and N is the dopant concentration. For example, for Si doped GaAs, with a room temperature electron concentration of 2 x 10^{17} cm^{-3}, the 1.51 eV donor peak width at 4K is 14 meV, i.e. about 30 times wider than the thermal limit. (See Appendix 2)

Other materials parameters can contribute to the broadening, eg. residual damage and strain after ion implantation and annealing.

In the case of impurity energy levels near mid band gap (deep levels) strong lattice coupling is common. This leads to strong phonon emission on recombination which causes a broad range of photon energies. The temperature dependence of this width is characteristic of the defect. An example is the work by Tajima (1985) on the EL2 defect in GaAs.

The peak energy is calculated from the measured wavelength in air, λ_{air}, by:-

$$E = h\nu = \frac{hc}{n_{air}\lambda_{air}} \quad (1)$$

where c = speed of light in vacuo, h = Planck's constant. A useful version is:-

$$E[eV] = \frac{1.2395}{\lambda_{air}[\mu m]} \quad (2)$$

for air at near infrared wavelengths. The refractive index of air, n_{air}, has been tabulated against wavelength (West, 1977). The peak energy is a function of the band gap of the semiconductor, so alloy compositions (e.g. in AlGaAs or in InGaAsP lattice matched to InP) can be determined. This is very useful for multilayered structures (e.g. lasers), where the composition of the thin, active, luminescence layer is required. CL methods separate the effects of the cladding layers, which have a larger band gap, unlike EDX or WDX. Active layers buried up to 3 µm deep can be excited with 30 keV electrons. Uniformity of the luminescence intensity, energy and peak width can be established non-destructively before expensive device processing. In very thin quantum well structures the energy upshift due to wavefunction confinement can be determined. This is a function of layer thickness, interface sharpness etc. (Skolnick et al, 1986).

In binary compound semiconductors the band gap at a given temperature is known (e.g. GaAs (Blakemore, 1974): 1.521 eV at 0K; 1.434 eV at 294K). At low temperature peaks of different energies can be resolved and these correspond to different impurity levels. The different chemical elements on the same site give different energies (e.g. at 4K in GaAs; using the notation of A° (or A^-) for a neutral (ionized) acceptor. An electron in the conduction band (e^-) recombines with a hole bound to an acceptor a) C°_{As}; 1.4935 eV, b) Si°_{As}; 1.4850 eV (Ashen et al, 1975)). This type of transition is notated as $(A^\circ,e^-) \rightarrow A^- + h\nu$ for acceptors in general or $(C^\circ,e^-) \rightarrow C^-_{As}$ + 1.4935 eV for carbon acceptors in GaAs specifically. The <u>same</u> element on a <u>different</u> site gives emission at different energies (e.g. at 4K in GaAs; $(Si^\circ_{As},e^-) \rightarrow Si^-_{As}$ + 1.4850 eV and $(Si^\circ_{Ga},h^+) \rightarrow Si^+_{Ga}$ + 1.5134 eV). Unfortunately there is a wealth of transitions in GaAs at around 1.51 eV and these are only resolvable in high purity samples at very low temperatures (2K), using resonant laser excitation. These include nearly all the shallow donor transitions $(D^\circ,h^+) \rightarrow D^+ + h\nu_1$, the free exciton transition $X = (e^-h^+) \rightarrow h\nu_2$, the bound exciton transitions e.g. $(D^\circ,X) \rightarrow D^\circ + h\nu_3$, $(A^\circ,X) \rightarrow A^\circ + h\nu_4$, $(D^+,X) \rightarrow D^+ + h\nu_5$ and the "two electron replicas" eg $(D^\circ,X) \rightarrow D^* + h\nu_6$ where the donor is not left in the ground state, D°, but in an excited state, D* (Skolnick et al, 1984; Almassey et al, 1981). This situation can be simplified in all but the purest samples by assuming that the 1.51 eV peak is mainly due to $(D^\circ,h^+) \rightarrow$

$D^+ + h\nu_3$. The chemical identity of the donor usually cannot be established by normal luminescence measurements.

Band-to-band transitions at low temperature, $(e^-,h^+) \rightarrow 1.521$ eV, are rarely observed because selection rules (which take conservation of momentum into account) favour exciton formation. (An exception is very heavily doped material.) At high temperatures, the near gap energy luminescence peak is too broad to be definitive about its origin, but the low exciton binding energy ($\sim$6 meV in GaAs) prevents exciton formation, and band to band transitions are usually observed.

Another commonly observed group of transitions are the donor-acceptor pair transitions $(D^\circ,A^\circ) \rightarrow (D^+,A^-) + h\nu$. The photon energy depends on the pair separation in the lattice. Usually the emission spectra of pairs of different separations merge into a broad CL peak. The peak energy increases with increasing excitation, because these conditions favour transitions involving close pairs, which emit at higher energy (Bergh and Dean, 1976a).

The energy liberated by radiative recombination can either emerge exclusively as a photon ("zero phonon line") or be shared between a photon and one or more phonons ("phonon replica line"). In the latter case the observed "phonon replica" photon has a lower energy than in the "zero phonon" case, by the amount required to create the appropriate phonon(s).

Indirect band gaps and deep level transitions favour phonon replica emission, but this type of luminescence can also be seen from shallow levels in direct gap material (e.g. in GaAs, the longitudinal optical (LO) phonon replica of the $(C^\circ_{As},e^-) \rightarrow C^-_{As} + 1.494$ eV transition (4K) is $(C^\circ_{As},e^-) \rightarrow C^-_{As}$ + LO (36 meV) + 1.458 eV).

In very heavily doped material with a small density of states in the majority band (eg the conduction band in n-type GaAs or InP) band filling effects are observed in the luminescence spectra. Electron states high in the conduction band become occupied at these dopant concentrations, an effect first noted in absorption measurements in InSb and known as the Moss-Burstein shift. In luminescence, the broad band-to-band peak increases in energy with increasing majority carrier concentration (n). The upshift ΔE is proportional to $n^{2/3}$. This change in energy is useful for determining high carrier concentrations by luminescence. An example in Ge doped InP is given later in the present paper.

A comprehensive account of the physics of luminescence in the III-V compounds is given by Bergh and Dean (1976b) including nearly one thousand references!

Experimental Difficulties

In this section difficulties such as signal to noise ratios, ion beam damage, contamination, surface damage and spectral artifacts are discussed.

A typical CL image requires the acquisition of ~1/4 million pixels in a time consistent with the stability of the microscope and being able to see the image for optimization purposes. Typically 100s is the maximum feasible record time, although this has to be increased for slow detectors. This constraint makes the optimization of signal-to-noise ratio a priority in the design and operation of an SEM-CL system. Better performance is obtained by use of LaB_6 high brightness electron guns, low aberration electron lens (by selection of an SEM with good lens performance and use of short working distances), high accelerating voltages (which increase gun brightness and decreases surface recombination rate), low noise (cooled) detectors and efficient collection optics. These features should be considered when choosing a performance/cost compromise. The use of high voltages leads to poor spatial resolution and ultimately beam damage (although not for the voltages available in most SEMs i.e. less than 50 kV). The signal-to-noise performance is less critical in moderately doped material, in direct gap semiconductors, for material with large gaps and therefore efficient detectors, in material with low concentrations of non-radiative centres, at low temperatures (where luminescence is favoured), and in experiments where a large wavelength band pass is acceptable. In extreme circumstances parallel acquisition of spectra through detector arrays or interferometers may become necessary.

The CL intensity is a sensitive function of the state of the sample surface. Work damage caused during sample preparation, ion beam damage from the SEM column, and hydrocarbons deposited from the residual gas in the chamber and cracked by the electron beam can affect the CL intensity. Examples are shown in Figure 2. Figure 2a shows a dark circle of ion damage from the SEM electron column. The circular shape is the geometrical ion shadow of the final aperture. This damage can be eliminated by use of a second aperture higher up the column (e.g. a selected area channelling pattern aperture fitted to some SEMs). The ion path is, in general, different from the electron one, so the ions are blocked but not the electrons. The second aperture has the additional advantage of preventing filament light from entering the CL optics. Figure 2b shows surface scratches (S) and a dark square caused by enhanced surface recombination after rastering the electron beam over the surface. This effect is strongest in low doped specimens, where the surface charge causes a deep depletion region whose electric field attracts injected carriers to the surface where they recombine non-radiatively. White squares can occur if surface repulsion dominates. The effect is negligible in heavily doped samples, e.g., in Fig 2c, which received the same dose of electrons as the undoped sample in Fig 2b (the horizontal bands in Fig 2c are due to genuine inhomogeneities in the material called dopant striations). The effect can be eliminated by preventing the surface charging; by application of one of the thin conductive coatings commonly used in SEM specimen preparation, e.g. sputtered gold. A very thin coat (~50Å) is required to allow the CL to escape.

The effect of self absorption in producing artifacts is important in CL systems with a large field of view in the collection optics. Such a

field of view, useful for low magnification images, allows multiple ray paths. This "ghost peak" phenomena, in relation to SEM-WDCL, has been appraised (Warwick and Booker, 1983 and Warwick, 1986).

Germanium Dopant Striations in Czochralski-Grown InP

A requirement for n^+ InP melt-grown substrates for InGaAsP layer growth can best be met by Ge doping. Ge doping hardens the lattice without precipitation (Brown et al 1981; Williams et al, 1982) (unlike Sn) and this leads to dislocation-free material suitable for low leakage-current detectors and long life lasers. Ge has a low diffusion coefficient (unlike S) and so does not auto dope the "intrinsic" layer of p-i-n detectors. However, Ge has a segregation coefficient (the ratio of Ge concentration in the solid InP to Ge concentration in the liquid InP) about a hundred times less than the ideal value of 1. This makes this material system prone to the occurrence of dopant striations. These are spatially periodic fluctuations in the dopant concentration caused by thermally driven periodic fluctuations in the growth rate.

Warwick and Booker (1983) showed that accurate determination of Ge concentration could be made by taking account of multiple reflected light paths and self-absorption resulting from a large collection optic field of view. Both CL peak width and band filling shifts were used and a good correlation between the methods obtained.

Changes in dopant concentration as small as 0.03 parts per million (atomic) were determined, with a spatial resolution of $\sim$3 μm. The determination of the magnitude of fluctuation against radial position in the substrate enabled the origin of the growth rate fluctuations to be determined (Warwick, 1983). The magnitude of the fluctuation as a function of mean dopant concentration was compared with melting point depression theory and a qualitative agreement found (Warwick, 1983). By comparing crystals grown with different crucible rotation rates it was found that these inhomogeneities could be minimized (Warwick, 1983; Warwick et al, 1983).

Schottky-Gated Field Effect Transistors in GaAs

These transistors have been fabricated using two types of GaAs material. These are the melt-grown undoped semi-insulating GaAs produced by the liquid encapsulated Czochralski (LEC) method and buffer layers grown by epitaxy. In the present case the epitaxial growth method was metal organic vapour phase epitaxy (MOVPE).

Material at three stages in the device process was studied; as received material, material with an activated sheet implant and that with lithographically defined implants in individual, electrically tested transistors. The object was to assess the homogeneity of the material and the effect of this on sheet implant and device uniformity (Warwick and Brown, 1985; Warwick et al, 1985).

Undoped semi-insulating (SI) LEC GaAs ingots contain two main point defects; carbon at a concentration of 10^{15} to 10^{16} cm^{-3} and the EL2 As_{Ga} related, deep donor defect at a concentration of 2 x 10^{16} cm^{-3}. The close compensation of C with EL2 is responsible for the desired SI properties. In addition, the material contains shallow donors (possibly S and Si) at a concentration of $\sim 10^{15}$ cm^{-3} and an As excess (or alternatively, a Ga deficiency) with, typically, a deviation of 2 x 10^{18} atoms cm^{-3} from the exact stoichiometric situation. Little is known about the excess As, most of which appears to be electrically inactive.

These ingots also contain extended defects, namely cellular polygonized arrays of dislocations, decorated with As precipitates. The precipitates account for only 10^{17} cm^{-3} excess As atoms, at most. The mean dislocation density is 10^4 to 10^5 cm^{-2} but varies locally. It is very high ($\sim 10^6$ cm^{-2}) on the arrays, which form the cell walls, but lower in the cell centres (10^2 to 10^3 cm^{-3}). The dislocations and point defects interact strongly during the cooling down period after solidification. In SEM CL, this interaction leads to the bright bands $\sim$20 μm wide along the arrays or cell walls, as marked W in figure 3b. Figure 3a shows an x-ray topograph of the same area, with the diffraction contrast revealing the dislocation arrays. The origin of the CL contrast is complex and presently not well understood despite much attention (Kikuta et al, 1984; Warwick and Brown, 1985; Chin et al, 1984; Wakefield et al, 1984). However there is agreement that the non-uniformity is severe. Several groups have established that sheet implant and device uniformity are not affected by dislocations themselves but by the inhomogeneous point defect distributions around them. This redistribution is activated by the high temperature of the GaAs LEC process (melting point 1238°C) (Warwick et al, 1985; Nakamura et al, 1985). Low temperature (700°C) MOVPE grown GaAs, containing dislocation arrays replicated from the substrate, have been shown to give uniform sheet implants (Warwick et al, 1985) and devices (Nakamura et al, 1985). The activation of the implant under the influence of the point defect concentration is the key to the link between substrate and device uniformity.

The critical device parameter is the threshold voltage. This is affected by the electron concentration in the transistor channel region. This is, in turn, determined by the implant activation efficiency. In LEC material, devices fabricated on cell walls show lower (more negative) threshold voltage than those on cell centres (Nakamura et al, 1985). This corresponds to more complete activation of the channel implant, if non-uniform activation is the cause of the difference.

SEM-WDCL at low temperatures shows a strong correlation of narrow 1.51 eV donor peaks for lower threshold voltages and broader peaks for higher ones (Warwick and Kitching, unpublished results). This result is somewhat surprising since one might expect a higher degree of activation to correspond to a broader CL peak on the principle of Mott broadening. The explanation appears to lie in the importance of broadening due

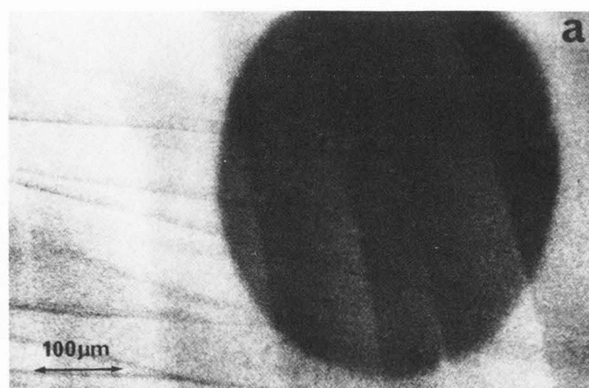

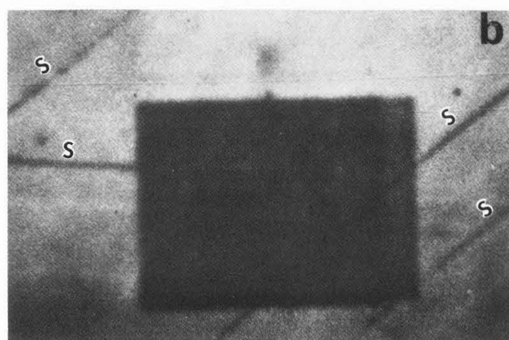

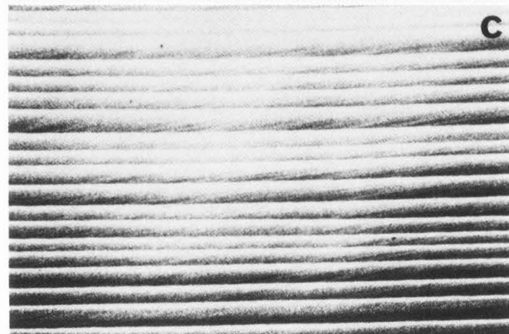

Figure 2a. SEM CL micrograph of ion bombardment damage in InP:Ge. The dark circle corresponds to the area under the SEM final aperture during the 3 minute exposure period.

Figure 2b. SEM CL micrograph of the dark square due to surface contamination in undoped InP. Same magnification as figure 2a. (Dark lines are due to scratches.)

Figure 2c. SEM CL micrograph of InP doped with 1.0×10^{19} Ge atoms cm^{-3}. The central region received the same electron dose as the sample in figure 2b but no dark square is seen. The high carrier concentration prevents the contamination-induced depletion dead layer. Same magnification as figure 2a. (The bright and dark bands are dopant striations.)

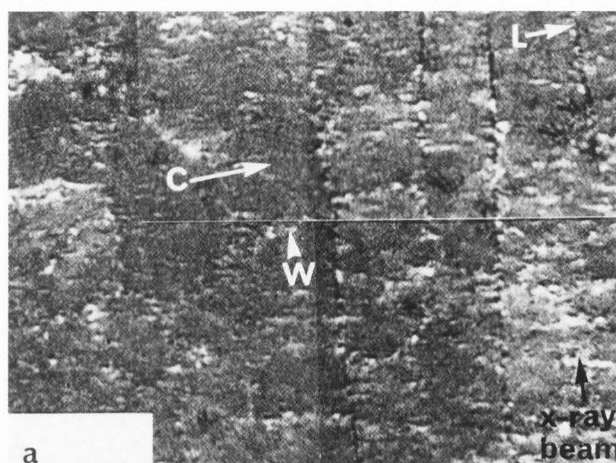

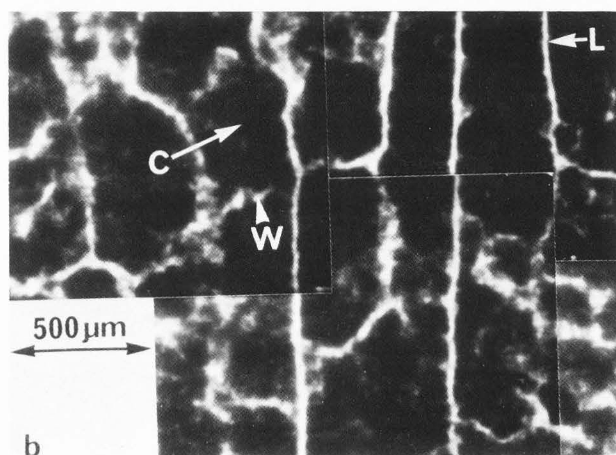

Figure 3a. Reflection x-ray topograph of the cellular dislocation arrays in undoped semi-insulating GaAs. Same magnification as figure 3b. C is a cell centre, L a lineage and W a cell wall.

Figure 3b. SEM CL image of the same area as 3a. The luminescence is from the 1.51 eV donor related transition. Points C, L and W are the same as figure 3a.

to stress or damage remaining from the implant. One possibility is that damage is more difficult to anneal out in areas close to the cell centres due to their point defect atmosphere.

Future Directions

Yacobi and Holt (1986) have noted that prophecy is profitless, but there is general agreement about the direction in which the SEM CL technique is moving; toward quantification. This must come about through the demonstration of the widespread applicability of quantified SEM CL methods, and consequent commercial availability of a low temperature SEM-TDWDCL package with MAS correction software. The technique could then become as widely used as SEM-WDX or SIMS.

Acknowledgement

Some of the work in this paper was supported by SERC(UK). It is a pleasure to acknowledge my colleagues who have promoted my own understanding of luminescence during many discussions. In particular, I warmly thank Dr DB Darby, Dr MM Al-Jassim and Dr GR Booker of the University of Oxford, Dr SM Davidson of UMIST and Dr MS Skolnick, Dr DR Wight and the late Dr PJ Dean of Royal Signals and Radar Establishment.

Appendix 1

A simple example serves to illustrate the competitive nature of luminescence. Figure A1 illustrates the energy band diagram of p-type material with two types of acceptor (A_2 and A_3) and figure A2 shows the spectrum from the three processes:- band to band (which is weak in general) and $(A_2^\circ,e^-) \rightarrow A_2^- + h\nu_2$ and $(A_3^\circ,e^-) \rightarrow A_3^- + h\nu_3$.

In a more general case there are j recombination channels (radiative and non-radiative) and each recombination channel, i, has a recombination rate

$$R_i = a_i c_i n \quad (3)$$

where n is the injected minority carrier density. This rate holds when the rate limiting step for each channel is determined by minority carrier capture and not majority carrier capture $(A^-,h^+) \rightarrow A^\circ + h\nu'$. a_i is a constant for a given defect in the sample (dependent on capture cross-section etc) and c_i is the defect concentration.

The total recombination rate is

$$\sum_{i=1}^{j} R_i = n \sum a_i c_i \quad (4)$$

Consider two cases:-

1. Beam on: injection rate G: dynamic equilibrium Minority carrier density n_0

$$\text{ith rate} = R_{io} = n_0 a_i c_i \quad (5)$$

$$\text{then} \quad G = \sum R_{io} \quad (6)$$

$$\text{from (5)} \quad G = n_0 \sum a_i c_i \quad (7)$$

$$n_0 = \frac{G}{\sum a_i c_i} \quad (8)$$

2. Beam turned off at time t=0: the decay of ith channel intensity, $I_i(t)$, is observed ($I_i(t)$ is proportional to $R_i(t)$)

$$G = 0 \qquad -\frac{dn}{dt} = n(t) \sum a_i c_i \quad (9)$$

i.e.

$$n(t) = n_0 \exp(-t \sum a_i c_i) \quad (10)$$

Substitute in equation (3)

$$R_i(t) = a_i c_i n_0 \exp(-t \sum a_i c_i) \quad (11)$$

$$\text{measured decay constant} = \tau = (\sum a_i c_i)^{-1} \quad (12)$$

τ is a function of all the processes.

Substitute equation (8) in equation (12)

$$n_0 = G\tau \quad (13)$$

Substitute equation (13) in equation (5)

$$R_{io} = a_i c_i G\tau \quad (14)$$

G and a_i are constant but R_{io} is proportional to the dynamic equilibrium intensity, I_{io}

$$\boxed{\text{concentration } c_i \propto \frac{I_{io}}{\tau}} \quad (15)$$

In practice other effects such as majority carrier capture $(A^-,h^+) \rightarrow A^\circ + h\nu'$ and unequal decay times of each peak must be considered.

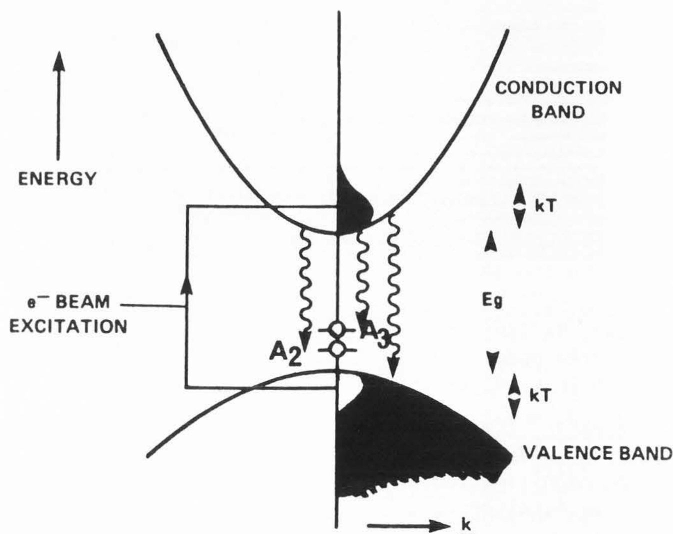

Figure A1. Schematic band diagram of electron energy, E, against wave vector, k. The forbidden gap E_g is marked. Two types of acceptor A_2 and A_3 are shown. The energy spread of electrons and holes is the product of Boltzmann's constant k and absolute temperature T. See Appendix 1.

Appendix 2

Shallow energy levels, the chemical shift and Mott broadening.

The photon energy on recombination for a carrier bound in the ground state of a shallow level is roughly the band gap plus the average thermal energy of the free carrier ($\sim$1/2 kT) minus the impurity binding energy. For a shallow defect the solution is pseudo-hydrogenic but the effective mass (m) of the ionized state must be used as well as the static dielectric constant $\varepsilon_r\varepsilon_o$ of the lattice.

Thus, neglecting the "chemical shift" (see below), the impurity "Rydberg energy" becomes

$$\frac{me^4}{32\pi^2\hbar^2\varepsilon_r^2\varepsilon_o^2} \qquad (16)$$

for GaAs, $\varepsilon_r \simeq 13$, the effective electron mass $m_e \sim 0.07 \times m_o$ and the effective hole mass $m_h \sim 0.51 \times m_o$, where m_o = free electron rest mass.

The donor ionization energy, E_D, is 5.7 meV and the acceptor ionization energy, E_A, is 41 meV. Compare this to the H atom ionization energy of 13.6 eV.

The Bohr radius a_o is

$$a_o = \frac{4\pi\varepsilon_r\varepsilon_o\hbar^2}{me^2} \sim 0.53 \text{ Å in hydrogen} \qquad (17)$$

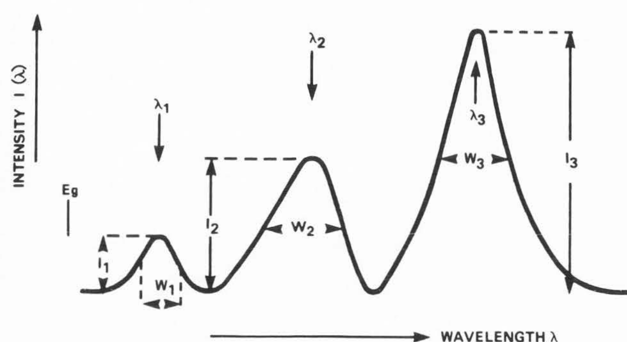

Figure A2. Schematic luminescence spectrum, showing the intensity I(λ) against wavelength λ, of the situation in figure A1. The peak at λ_1 corresponds to band to band transitions. It has peak intensity I_1 and width ω_1. Similarly λ_2, I_2 and ω_2 refer to the $(A_2^\circ,e^-) \rightarrow A_2^- + \frac{hc}{n_{air}\lambda_2}$ transition and λ_3, I_3 and ω_3 to that for A_3. See figure A1 and Appendix 1.

For a donor, the effective Bohr radius is about 100 Å ($\sim$17 times lattice parameter). For an acceptor it is about 13 Å ($\sim$2.4 times lattice parameter).

Thus, the difference in effective masses of carriers in the valence and conduction bands gives rise to different donor and acceptor behaviour. The electron bound to a donor "sees" very little of the disturbance due to the donor itself. This disturbance, called the chemical shift, is very small for donors ($\sim$0.3 meV), because of the very wide Bohr radius. It is larger in acceptors ($\sim$9 meV) because of the smaller radius. As the name implies this modification to the Rydberg energy, due to the disturbance of the lattice is chemical species dependent. The chemical shift for different donors is very difficult to resolve spectroscopically.

At moderate donor concentrations the wide Bohr radius of the donor-bound electron wave-functions overlap and broaden the ground state energy. This is Mott broadening and is inversely proportional to mean impurity separation and thus proportional to $N^{1/3}$ where N is the impurity concentration. The Mott broadening parameter is $\beta = aN^{1/3}$, where a is the effective Bohr radius. At helium temperatures the broadening is significant for $\beta > 0.24$ (the Mott criterion). Thus for GaAs with only shallow donors, N_D has to be less than 1.4×10^{16} cm^{-3} for no broadening. For the case of only shallow acceptors, N_A has to be less than 6×10^{18} cm^{-3}. In compensated material the broadening is roughly additive even though the measured carrier concentration is the difference of the donor and acceptor concentrations. An additional complication in compensated material is the family of energy levels from donor-acceptor pairs of different separations.

References

Almassy RJ, Reynolds DC, Litton CW, Bajaj B, McCoy GL. (1981). Observation of shallow residual donors in high purity epitaxial GaAs by means of photoluminescence spectroscopy. Solid State Commun. 38 1053-1056.

Ashen DJ, Dean PJ, Hurle DTJ, Mullin JB, White AM, Greene PD. (1975). The incorporation and characterization of acceptors in epitaxial GaAs. J.Phys.Chem.Solids 36 1041-1053.

Bergh AA, Dean PJ. (1976a). Light emitting diodes, Clarendon Press: Oxford, 82-86.

Bergh AA, Dean PJ. (1976b). ibid, 69-342.

Blakemore JS. (1974). Solid State Physics, WB Sanders:Philadelphia, 306.

Brown GT, Cockayne B, MacEwan WR. (1981). The growth of dislocation free Ge-doped InP. J.Crystal Growth 51 369.

Chin AK, Caruso R, Young MSS, Von Neida AR. (1984). Uniformity characterization of semi-insulating GaAs by cathodoluminescence imaging. Appl.Phys.Lett. 45, 552-554.

Crookes W. (1879). On the illumination of lines of molecular pressure and the trajectory at molecules (1879). Phil.Trans.Roy.Soc. (London) Part 1 1879 135-164.

Hastenrath M, Kubalek E. (1982). Time-resolved cathodoluminescence in scanning electron microscopy. Scanning Electron Microsc. 1982; I: 157-173.

Hwang CJ. (1972). Quantum efficiency and radiative lifetime of the band to band recombination in heavily doped n-type GaAs. Phys.Rev. B6 1355-1359.

Kamiya T, Wagner E. (1977). Optical determination of impurity compensation in n-type gallium arsenide. J.Appl.Phys. 48 1928-1934.

Kikuta T, Katsumata T, Obokata T, Ishida K. (1984). Microscopic distribution of deep and shallow levels around dislocations in undoped SI-GaAs. Inst.Phys.Conf.Ser. (Adam Hilger: Bristol) No 74 47-52.

Kyser DF, Wittry DB. (1964). The electron microprobe (T.D. McKinley. K.F.J. Heinrich and D.B. Wittry (eds)) Wiley, New York, pp 691-714.

Nakamura H, Matsuura H, Egawa T, Sano Y, Ishida T, Kaminishi K. (1985). Characterization of microscopic uniformity of semi-insulating GaAs substrate by using high density FET array. Extended Abstracts of the 17th Conference on Solid State Devices and Materials, Tokyo 1985, 429-432.

Nam SB, Langer DW, Kingston DL, Luciano MJ. (1977). Determination of concentrations of donors and acceptors by an optical method. Appl. Phys.Lett. 31 652-654.

Pickering C, Tapster PR, Dean PJ, Ashen DJ. (1983). Determination of impurity concentration in n-type InP by a photoluminescence technique. Inst.Phys.Conf.Ser. (Adam Hilger:Bristol) No 65 469-476.

Skolnick MS, Harris TD, Tu CW, Breman TM, Sturge MD. (1984). Strongly polarised bound exciton luminescence from GaAs grown by molecular beam epitaxy. Appl.Phys.Lett. 46 427-429.

Skolnick MS, Tapster PR, Bass SJ, Apsley N, Pitt AD, Chew NG, Cullis AG, Aldred SP, Warwick CA. (1986). Optical properties of InGaAs-InP single quantum wells grown by atmospheric pressure metal-organic chemical vapour deposition. Appl.Phys.Lett. 48 1455.

Swaminathan V, Von Neida AR, Caruso R, Young MS. (1982). Photoluminescence evaluation of semi-insulating GaAs grown by the liquid encapsulated Czochralski technique. J.Appl.Phys. 53 6471-6474.

Tajima M. (1985). Deep level photoluminescence commonly present in undoped Czochralski-grown GaAs. Appl.Phys.Lett. 46 484-486.

Wakefield B, Leigh PA, Lyons MH, Elliot CR. (1984). Characterization of semi-insulating liquid encapsulated Czochralski GaAs by cathodoluminescence. Appl.Phys.Lett. 45 66-68.

Warwick CA. (1983). Defects in Czochralski-grown InP and GaAs ingots. Doctoral Thesis. University of Oxford.

Warwick CA, Booker GR. (1983). Use of SEM CL spectra to determine local variations in Ge doping concentration in LEC InP ingots. Inst.Phys.Conf. Ser. Adam Hilger:Bristol 67, 321-326.

Warwick CA, Brown GT, Booker GR, Cockayne B. (1983). Dopant inhomogeneity in Czochralski-grown indium phosphide ingots doped with germanium. J.Crystal Growth 64, 108-114.

Warwick CA, Brown GT. (1985). Spatial distribution of 0.68 eV emission from undoped semi-insulating gallium arsenide revealed by high resolution luminescence imaging. Appl.Phy.Lett. 46 574-576.

Warwick CA, Gill SS, Wright PJ, Cullis AG. (1985). Spatial variation of dopant concentration in $^{29}Si^{+}$ implanted Czochralski and metal organic vapour phase epitaxial GaAs. Inst.Phy.Conf.Ser. Adam Hilger:Bristol 76, 365-372.

Warwick CA. (1986). Common occurrence of distortion in semiconductor luminescence spectra. J.Appl.Phys. 59, 4182-4184.

West RC (ed). (1977). Handbook of Chemistry and Physics 55th Edition, Chemical Rubber Company Press: Cleveland, E223.

Williams JO, Crawford ES, Brown GT, Cockayne B. (1982). High resolution transmission electron microscopy of InP. J.Mat.Sci.Lett. 1 499-502.

Yacobi BG, Holt DB. (1986). Cathodoluminescence scanning electron microscopy of semiconductors. J.Appl.Phys. 59 R1-R24.

Discussion with Reviewers

A. Jakubowicz: You write that dark and white squares appearing after scanning the electron beam over the surface can be eliminated by preventing the surface charging by application of a thin conductive coating. If so, one should not observe such squares in the EBIC mode either, when Schottky contacts are used for charge collection. Could you explain the presence of dark and white squares in the EBIC mode?

Author: In my experience with CL mode the squares can always be eliminated by the surface conductor method. There may be other causes of squares in CL and/or EBIC mode of other SEMs which are outside my experience. These other causes may not be curable by the surface conductor method. My colleague, P R Wilshaw, informs me that, in an SEM with a "clean" vacuum system, no scan squares are observed in EBIC mode, even after prolonged scanning of tens of hours on the same small area.

A. Jakubowicz: As you mentioned, quantification of the CL technique requires knowledge of lifetimes. Could you comment on the chances of quantifying the CL method in non-uniform materials, in which the locally measured decay times depend not only on the number of recombination centres, but also, for example, on their geometrical configuration, and presence of electrical barriers at extended defects?

D. Köhler: The concentration of radiative centres is only one of several factors which affect intensity, the spatial distribution and the transient behaviour of cathodoluminescence. The position and strengths of defects and internal electric fields etc may often be important. Do you believe that the applicability of a MAS correction program will not be restricted to a few special cases?

Author: I believe one is better off knowing the local decay time than not knowing it. The accuracy and applicability of a MAS correction program will, like ZAF programs for EDX/WDX and matrix-effect programs for SIMS, be limited by the sophistication of the physics in the software. As this improves so will the usefulness.

D. Köhler: Your detection system covers a broad range from 0.3 μm to 5.5 μm. Can you give any figures about the loss in your system?

Author: Reflection loss at the Al coated parabola is 15% at 800 nm. About 25% is lost through the electron beam hole and due to the finite solid angle of the parabola (for a Lambertian source). At the parabola focus, the parallel component of the beam from the parabola passes down the hollow light guide with no loss, but for off-axis points a loss of less than 5% per grazing reflection at the Ag coating on the inside of the tube is suffered. For a point 100 μm from the parabola focus 2 to 3 reflections occur. The sapphire window has a transmission of better than 90% for 600 nm to 4 μm and 70% at 5.5 μm. The CaF lens has better than 90% transmission from 200 nm to 7 μm. The 45° mirror, for total light mode, is Al coated and so a 15% loss is suffered (total light mode only). However, the principal source of loss is due to aberrations in the parabola. This leads to a non-diffraction limited blur spot about 1 mm diameter at the spectrometer slits. When using high spectral resolution much light is cut out by narrow slits. In total about 30% of the Lambertian (cosine) emission from a planar sample at the parabola focus is delivered into 500 μm wide slits (about 3 nm resolution). Further loss occurs at the two reflection lenses and at the grating in the monochromator, with a peak transmission at the blaze angle, of 30% for randomly polarized light in an f4 cone (i.e. no overfilling of the grating). We have four blazed gratings with peaks at 500 nm, 1 μm, 2 μm and 4 μm. The gratings have a useful range of 0.6 to 1.5 times the blaze wavelength.

D.Köhler: Can you give further information concerning the ion beam?

Author: I have no measurements on my SEM but I understand from my colleague D.J. Robbins that electron columns commonly produce negative ion beams by ionization and acceleration between the gun anode and cathode. Common ions are H^-, C^-, O^-, N^-, W^- for W filament guns. Presumably La^- and B^- would be found in LaB_6 guns additionally.

D. Köhler: In table 3 it is mentioned that no materials that scintillate are used. What kind of electron detector do you use?

Author: The electron detector is not used in the CL mode. It may be removed from the SEM chamber if it is a problem. However, our Thornley-Everhart electron detector is outside the field of view of the CL optics and can be left in position without a scintillation problem.

D. Köhler: Working in our laboratory with IR detectors we sometimes get a serious problem with a strong background signal due to reflected light from the cathode. Do you observe this too? How do you overcome this problem?

Author: Yes, there is filament light which we exclude by two methods. Firstly, our SEM is fitted with an adjustable aperture, 100 μm in diameter, between the second and final lenses. We use this, in addition to the final lens aperture (400 μm diameter), as an adjustable, small diameter spray aperture to block the light. It does not degrade the probe performance noticeably. It was originally designed for use without the final aperture for selected area channelling patterns. It also removes the ion beam. Secondly we use phase sensitive (lock-in) detection with electrostatic electron beam blanking. Thus the CL is modulated but any residual filament light or thermal radiation is constant and so it is excluded from the lock-in output.